Retarding field energy analyser ion current calibration and transmission

Retarding field energy analyser ion current calibration and transmission

2011 J. Phys. D: Appl. Phys. 44 075205

(http://iopscience.iop.org/0022-3727/44/7/075205)

IOP PUBLISHING JOURNAL OF PHYSICS D: APPLIED PHYSICS

J. Phys. D: Appl. Phys. **44** (2011) 075205 (7pp) doi:10.1088/0022-3727/44/7/075205

Retarding field energy analyser ion current calibration and transmission

K Denieffe[1], C M O Mahony[1], P D Maguire[1], D Gahan[2] and M B Hopkins[2]

[1] N.I. Biomedical Engineering Centre, Nanotechnology Research Institute, University of Ulster, BT 37 0QB, Northern Ireland

[2] National Centre for Plasma Science and Technology, Dublin City University, Glasnevin, Dublin 9, Ireland

Received 21 July 2010, in final form 16 November 2010
Published 2 February 2011
Online at stacks.iop.org/JPhysD/44/075205

Abstract

Accurate measurement of ion current density and ion energy distributions (IEDs) is often critical for plasma processes in both industrial and research settings. Retarding field energy analysers (RFEAs) have been used to measure IEDs because they are considered accurate, relatively simple and cost effective. However, their usage for critical measurement of ion current density is less common due to difficulties in estimating the proportion of incident ion current reaching the current collector through the RFEA retarding grids. In this paper an RFEA has been calibrated to measure ion current density from an ion beam at pressures ranging from 0.5 to 50.0 mTorr. A unique method is presented where the currents generated at each of the retarding grids and the RFEA upper face are measured separately, allowing the reduction in ion current to be monitored and accounted for at each stage of ion transit to the collector. From these I–V measurements a physical model is described. Subsequently, a mathematical description is extracted which includes parameters to account for grid transmissions, upper face secondary electron emission and collisionality. Pressure-dependent calibration factors can be calculated from least mean square best fits of the collector current to the model allowing quantitative measurement of ion current density.

(Some figures in this article are in colour only in the electronic version)

1. Introduction

Accurate measurements of ion energy distributions (IEDs) and ion current densities (J_i) of plasma discharges and ion beam sources are important for optimization and control of thin-film deposition and etching processes and the design of plasma sources. In the case of deposition, the ion bombarding energy and flux have a direct effect on the deposition rate and properties of the resulting film [1]. We recently reported detailed mass spectrometry, mass selected ion energy and flux measurements during the growth of carbon-based films [2]. However use of complex mass–energy analysis (MEA) instrumentation is problematic in many plasma processing environments. There is also an increasing demand for accurate *in situ* control sensors for etch processes used in the manufacture of magnetic data storage devices and silicon wafer technologies as these industries move to ever-reducing critical dimensions [3]. The small size and low cost of retarding field energy analysers (RFEAs) compared with other IED measurement tools mean that it is a useful diagnostic device for both industrial process control and basic research. Compared with MEA these devices are much less complex and do not require differential pumping in applications below 100 mTorr [4]. In addition RFEAs have also been used to measure electron energy distribution functions (EEDFs) by other groups [4]. To date, RFEAs have been used mainly for IED measurement [5–9], with only limited application to *in situ* determination of ion flux density [10] due to the lack of a clear consensus on how best to calibrate its ion current density measurements. Here we describe the calibration of current measurements made with an RFEA. In a second publication [11] we report the sputter yields of thin film ferrous alloys in an argon ion beam facility based on our calibrated RFEA.

An RFEA is essentially a stack of electrically isolated grids and an ion collector, all positioned along the ion beam path. Selectable potentials can be applied to the grids to reject beam plasma electrons, to allow energy analysis and to suppress internal secondary electron (SE) emission before

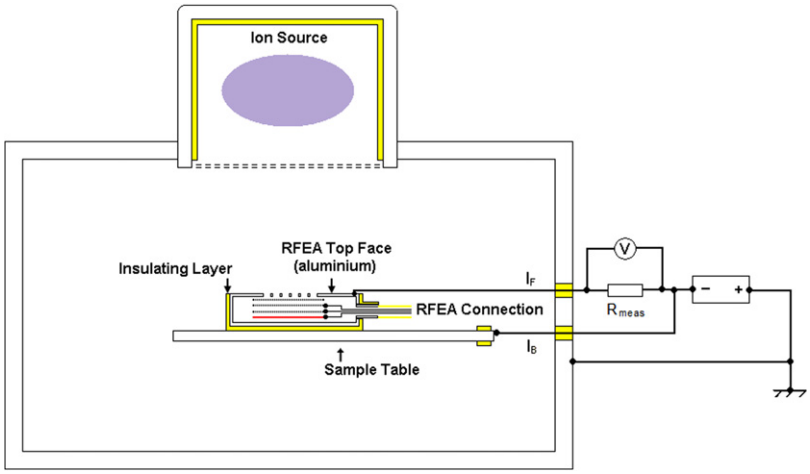

Figure 1. Experimental schematic showing RFEA top face exposed to ion beam.

ion collection. When RFEAs are used to measure an IED, an ion retarding potential is applied to a grid to separate ions arriving at the RFEA entrance aperture plane by kinetic energy. As the retarding potential is varied, ions of different energies are reflected, or transmitted to subsequent grids for collection. It could be assumed that at low pressures, charged particle flux can be estimated from the product of the known optical transmission of each grid. This approach is, however, only valid for collisionless trajectories at low pressures [12], typically below 1 mTorr for the shallow (∼1 mm deep) RFEA used in this study, and for uniform fluxes incident at *each* grid, i.e. relatively straightforward ion optics. Another alternative calibration technique is to compare RFEA ion currents with a reference ion flux, determined from a separate Faraday cup or Langmuir probe measurement. The latter technique has been used by Gahan *et al* [4] to compare the RFEA flux determined from RFEA collector current and assumed transmission to the probe saturation ion current and the Bohm flux determined from the probe I–V and extracted values of N_e and T_e. While RFEA and Langmuir ion current characteristics exhibit similar trends, decreasing markedly with pressure, the accuracy of the comparison is limited by standard Langmuir probe design and analysis methods. Baloniak *et al* [13] performed a calibration of the measured ion collector current (I_C) by modelling the total collisional (T_{CTOT}) and geometrical transmissions (T_{GTOT}) of a four-grid RFEA based on the Bohm current (I_B) at the RFEA orifice derived from Langmuir probe measurements with T_{CTOT} and T_{GTOT} as fit parameters ($I_C = T_{GTOT}T_{CTOT}I_B$). An additional method was used at a single pressure (7.5 mTorr) where T_{CTOT} was determined directly by comparing the ion current density at the RFEA top face to the ion current at the collector ($=e^{-L/\lambda}$, where L is the device length, λ is the ion mean free path). Reasonable consistency across the range 7.5–52.7 mTorr was obtained using best fit parameters $P_G = 2.23\%$ and cross-section $\sigma = 6.06 \times 10^{-15}\,cm^2$. This cross-section was also used to calculate the collisional transparency (P_C) in the additional method, which subsequently yielded a geometrical transparency of $P_G = 3.32\%$. It was suggested that uncertainty in the determination of N_e is likely to lead to an overestimate of the ion current to the orifice which may account for discrepancies in geometrical transparency determined from the two methods. There are several other factors limiting the calibration accuracy based on measuring the current at the top face. (i) The current density may not be uniform across the top face, depending on the plasma conditions. (ii) Differences in SE emission coefficient between top face and collector may be significant, even when the same material is used, since surface condition can have as great an impact as surface material [14]. Also, as the authors point out, the presence of a positive plasma sheath potential produces a preferred direction of the SEs away from the top face surface resulting in a larger SE emission at the top face compared with that at the collector. (iii) Collection of slow ions arriving at the reference electrode will further add to the current inventory. These ions originate from charge exchange collisions or from a diffuse beam plasma. The latter is produced by ionization via SEs released from surfaces or from ion–atom collisions.

In this study, we develop a technique which involves recording currents to each RFEA grid or the collector in turn as the specific potential to that grid is swept. The RFEA top face current is also recorded. The advantage of this method is that it allows the observation of the progressive reduction in measured current at each of the grids. This improves the analyses and hence accuracy of the calculated grid transmission values and the extracted SE emission of each grid. Also, full calibration can be performed with the RFEA *in situ* without needing a remote reference measurement of ion current, e.g. using a Langmuir probe.

2. Experimental configuration

All measurements were performed with a Copra GSE 160 ion beam source operated in a custom-built vacuum chamber. This consists of a 13.56 MHz plasma inductively coupled (ICP) source with a grounded extraction grid. Rf power is coupled to the plasma through a single turn induction coil and a source-incorporated matching network. The source was operated throughout at 200 W rf power and 5.4 sccm argon flow. The RFEA was positioned centrally on the sample table (figure 1) and the RFEA casing was separated electrically from the table

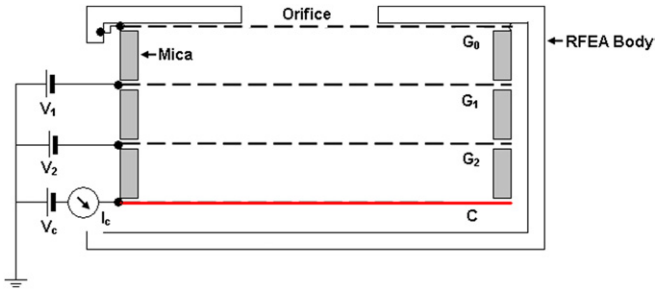

Figure 2. Cross-section of RFEA probe showing potentials applied to orifice and grids.

by an insulating holder which masked its base and sides; this allowed the current to its top face (I_F) to be measured distinctly from the table current (I_B). The RFEA top face area A_F was accurately defined by the insulating holder which prevented the ion beam striking its side.

The Copra ion source produces an ion beam extracted by a circular grounded extraction grid of 84 mm diameter. The extraction potential is provided by the ion source plasma potential V_{PLDC}, typically 10 to 20 V. A small number of fast electrons, with energy greater than V_{PLDC}, also exit the source, but are deflected to the vacuum wall by the biased sample table. The ICP source is operated at 200 W in the H mode and under these conditions the rf component of plasma potential V_{PLRF} is typically a few volts.

The RFEA was mounted on the biased sample table ($V_B = -50$ V) and a separate dc power supply was used to repel beam plasma electrons during calibration. I_F (figure 1) was measured outside the vacuum chamber across a resistor ($R_{meas} = 99.7\ \Omega$). The RFEA casing potential V_A is the sum of sample table potential and the small potential drop across R_{meas} ($V_A = V_B + V_{R_{meas}}$). The ion beam current density was found to peak on axis, is almost circularly symmetric, and reduces with distance from the source with a $\sim \pm 15^\circ$ divergence.

The vacuum chamber has a volume of ~110 litres pumped using a 140 l s^{-1} turbomolecular pump (TMP) that is backed using a 25 m^3 h^{-1} rotary pump. Chamber pressure control is achieved by adjusting chamber pumping, controlled by restricting the conductance pathway to the TMP with a throttle valve.

A cross-section of the RFEA (Impedans Ltd Semion^{TM} model [15]) used in this work is given in figure 2. It is coupled to a software interface to control the voltages applied to each of the grids and to provide graphical output of IEDs and grid ion currents. The aluminium RFEA outer casing (figure 2) has a diameter of 70 mm, its top face has 37 × 0.83 mm diameter orifices with a total ion acceptance area of 21.5 mm^2. The RFEA consists of three nickel grids (G_0, G_1 and G_2) laser machined to produce an array of square apertures and a copper current collector plate. The grids are 4 μm thick, each separated by 235 μm mica insulators. Figure 3 shows a scanning electron micrograph (SEM) of a sample of grid mesh. The optical transmission is the ratio of the open area of a grid to its total area. The RFEA mesh has open square apertures of sides L (~15 μm) each separated by solid metal of dimension S (~10 μm): giving an optical transmission factor (T_{OPT}) of

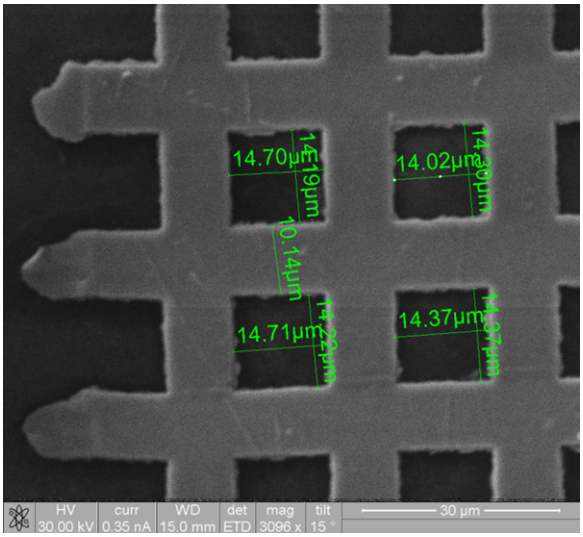

Figure 3. SEM image of a sample grid mesh. The sides of the square (L) are ~14–15 μm and solid metal (S) ~10 μm.

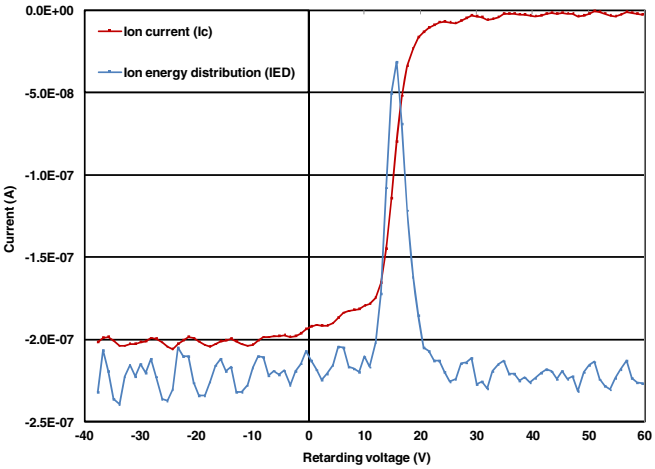

Figure 4. Typical RFEA measurement. The blue line shows subsequent IED obtained after differentiating data from I–V in the red line (1 mTorr, 200 W).

0.34. The total thickness of the RFEA is 5 mm and the distance from the top face apertures to the collector is 900 μm.

To measure IEDs, the RFEA is operated as follows: (i) ions pass through the orifice and first grid (G_0), both of which are at RFEA casing potential V_A.(ii) A varying potential V_1 is applied to the second grid, G_1, and swept in 0.1 V increments from −50 V dc to well above the ion source plasma potential (typically 10 to 20 V).

The potential V_1 on G_1 determines the proportion of ions transmitted. Those that possess energy greater than $e(V_A - V_1)$ pass through G_1 (and G_2) to the collector. G_2 is biased at −60 V dc to repel any electrons that enter the RFEA. (iii) The current collector plate is biased at −10 V, 50 V more positive than G_2, to ensure a net SE current does not leave the collector.

The output for a typical IED measurement is shown in figure 4. The I–V characteristic (red line) is differentiated to obtain the IED (blue), showing a narrow, almost, mono-energetic distribution peaking at ~16 eV. For $V_1 < -10$ V, all ions are accepted and the total flux is equivalent to ~200 nA.

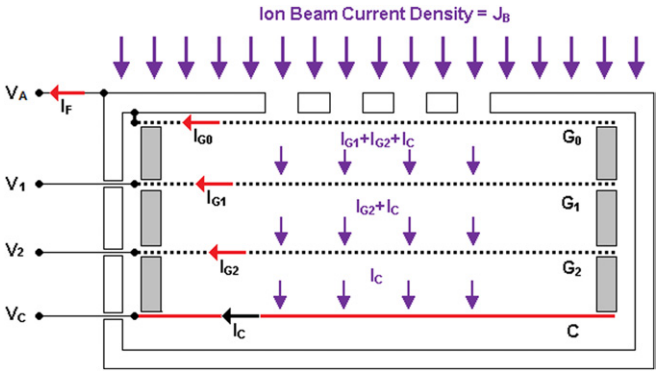

Figure 5. Cross-section of RFEA probe showing grid currents.

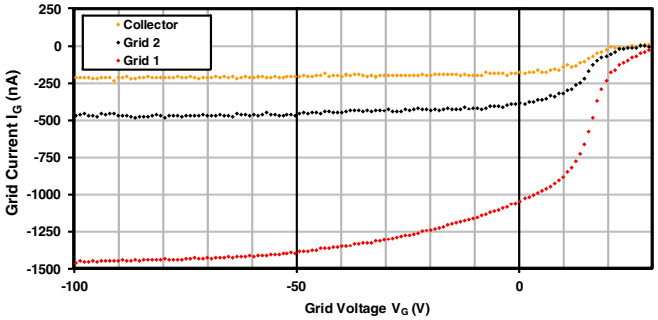

Figure 6. Ion current I–V plots at grid 1, grid 2 and collector for $P = 1$ mTorr.

3. RFEA calibration

A schematic cross-section of the RFEA is shown in figure 5 indicating the grids, voltages and currents used in the calibration process which relates the incident current density J_B to the measured collected current I_C, detailed later in the results section. Note that the ion current that passes through a grid is the sum of currents to all subsequent grids and the collector. Because only one RFEA channel at a time can be used to measure current, I_{G_1}, I_{G_2} and I_C were measured sequentially under the same ion beam conditions, I_F and other parameters were also recorded. To produce the current–voltage (I–V) plots shown in figures 6 and 7, the potential on each grid was swept from −100 V to +100 V whilst its grid current was measured. This procedure also allowed analysis of the ion beam current behaviour with retarding potential. Whilst a particular grid potential was being swept and its current measured, a potential equal to the RFEA casing potential, V_A (−50 V), was applied to the other grids. Two calibrations were performed: a low pressure calibration valid for $P \leqslant 1$ mTorr and a more general pressure-dependent calibration for 0.5 mTorr $\leqslant$ P $\leqslant$ 50 mTorr.

Figure 6 shows I–V plots for grids 1, 2 and the collector for grid voltages ranging from −100 to +100 V. Note that the RFEA PSU is configured such that supplied positive current to a grid is a positive value. Therefore, increasing positive ion flux arriving at an RFEA grid is measured as an increasingly negative current value.

Data were taken for pressures ranging from 0.5 to 50 mTorr and for all of the data sets of the following features

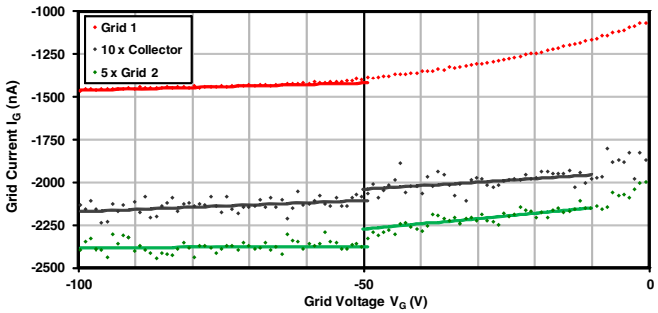

Figure 7. Example ion current extrapolations for figure 6 to determine I_{G_1}, I_{G_2}, I_C and SE emission coefficients. To aid viewing the collector current is magnified 10× and grid 2 by five.

were observed:

(i) From −100 V to ∼−50 V, the ion flux arriving at each grid is relatively constant.

(ii) For $-50\,\text{V} < V_G < -40\,\text{V}$, I_{G_2} and I_C increase by a small factor due to ion induced SE emission. This effect is seen more easily in the magnified view in figure 6 for the $5 \times I_{G_2}$ (green) and the $10 \times I_C$ (dark grey) data. It is just discernible in the I_{G_1} measurement.

(iii) For $-40\,\text{V} < V_G < 0\,\text{V}$, I_{G_2} and I_C are relatively constant; however, there is a marked increase in I_{G_1} with increasing V_G.

(iv) For $0\,\text{V} < V_G < 30\,\text{V}$, the variation of positive ion collection dominates, particularly for $10\,\text{V} < V_G < 20\,\text{V}$.

Values for I_{G_1}, I_{G_2} and I_C are determined by extrapolating (figure 7) the I–V plots for $-100\,\text{V} < V_G < -60\,\text{V}$ to $V_G = -50$ V, at which point there is no net field within the RFEA. At 1 mTorr, values for I_C (211 nA), I_{G_2} (475 nA) and I_{G_1} (1418 nA) were obtained. Less than 1% of ions undergo collisions within the RFEA at this pressure and hence their effect can be ignored. The measured current I_G to a grid contains contributions from the incident ion currents I_i striking the upper grid face and ion-induced SEs. These electrons escape from the upper grid face if its potential is lower than the previous grid. The current to the previous grid thus includes SEs from the upper face of the subsequent grid. In the absence of currents from other sources (e.g. ion–neutral collisions within the RFEA), the ion currents I_i are related to the measured current I_G and the ion induced SE emission coefficient, γ, by the following:

(i) If the grid potential is lower than the previous grid:

$$\text{Grid } G_1 \; I_{G_1} = I_{i1}(1 + \gamma_{Ni})$$
$$\text{Grid } G_2 \; I_{G_2} = I_{i2}(1 + \gamma_{Ni})$$
$$\text{Collector } I_C = I_C(1 + \gamma_{Cu}).$$

(ii) If the grid potential is higher than the subsequent grid:

$$\text{Grid } G_0 \; I_{G_0} = I_{i0} + \gamma_{Ni} I_{i1}$$
$$\text{Grid } G_1 \; I_{G_1} = I_{i1} + \gamma_{Ni} I_{i2}$$
$$\text{Grid } G_2 \; I_{G_2} = I_{i2} + \gamma_{Cu} I_{iC}.$$

For the collisionless case ($P \leqslant 1$ mTorr), the ion transmissions T_{G_1} and T_{G_2} of RFEA grids G_1 and G_2 are the ratio of the ion current that passes through that grid to the ion current incident

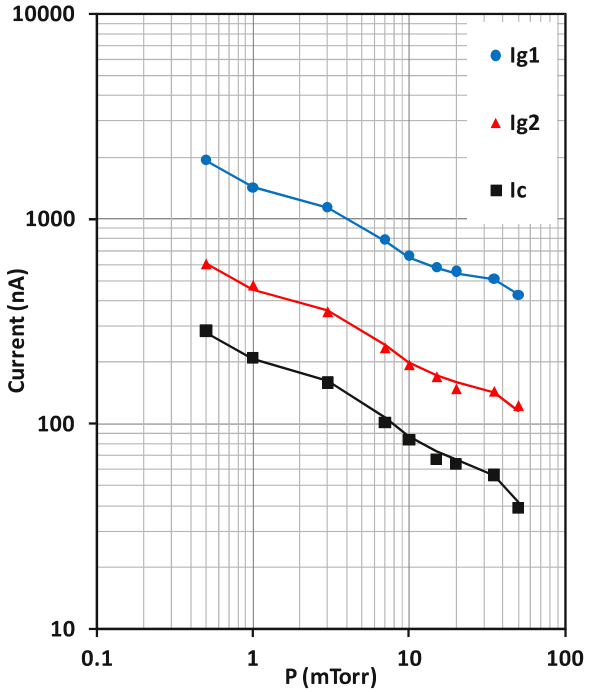

Figure 8. Pressure dependence of measured grid currents I_{G_1}, I_{G_2} and I_C.

I_i upon it. The calculated values are 0.33 and 0.31 for T_{G_1} and T_{G_2}, respectively, from

$$T_{G_1} = \frac{I_{i2} + I_{iC}}{I_{i1} + I_{i2} + I_{iC}}, \qquad T_{G_2} = \frac{I_{iC}}{I_{i2} + I_{iC}}.$$

The current I_{G_0} to grid G_0 cannot be measured directly in the same manner as I_{G_1}, I_{G_2} and I_C because grid G_0 is electrically connected to the RFEA top face which also collects a much larger current. However, if a constant ion current density is assumed across the top face, I_{G_0} can be estimated from the relative areas of the upper face and the grid G_0. When this estimate of I_{G_0} is used to calculate grid G_0 ion transmission T_{G_0}, a value of 0.24 is obtained. This value suggests a significantly lower transmission than both the optical (0.34) and the calculated transmissions for grids G_1 ($T_{G_1} = 0.33$) and G_2 ($T_{G_2} = 0.31$). This is expected to be largely due to an overestimate of the ionic component of I_F, the RFEA face current due to SE emission from the RFEA top face as well as collection of ions from beam plasma and charge transfer collisions above the RFEA. Moreover, it may be affected by a limited RFEA angular ion acceptance and the ion optical effects at grid G_0.

3.1. Calibration in the pressure range 0.5–50 mTorr

The pressure dependences of the grid currents determined by the method outlined in this section are shown in figure 8 and a detailed analysis of current inventories was carried out (figure 9) to determine the components of these currents.

$$I_{G_1} = I_A T_{G_0}[T_{GAP}(1 - T_{G_1}) + \tfrac{1}{2}(1 - T_{GAP}) + \tfrac{1}{2} T_{GAP} T_{G_1}(1 - T_{GAP})] \quad (1)$$

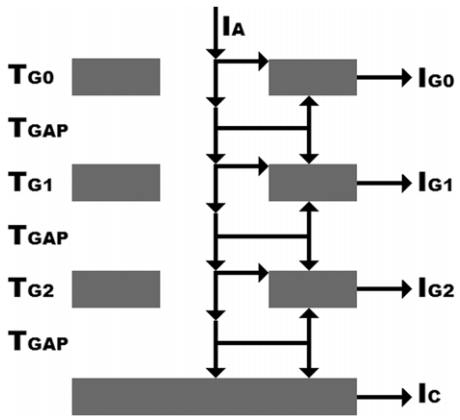

Figure 9. Current inventories showing components of grid currents I_{G_0}, I_{G_1}, I_{G_2} and I_C.

$$I_{G_2} = I_A T_{G_0} T_{G_1} T_{GAP}[T_{GAP}(1 - T_{G_2}) + \tfrac{1}{2}(1 - T_{GAP}) + \tfrac{1}{2} T_{GAP} T_{G_2}(1 - T_{GAP})] \quad (2)$$

$$I_C = I_A T_{G_0} T_{G_1} T_{GAP}^2 \left[T_{GAP} + \tfrac{1}{2}(1 - T_{GAP})\right]. \quad (3)$$

The measured currents I_{G_0}, I_{G_1} and I_{G_2} are shown in figures 5 and 9. I_A was calculated from the measured current to the RFEA top face (I_F), the area of the face A_F, the open area of the 37 apertures A_2, and an assumed top face SE emission coefficient γ

$$I_A = \gamma I_F \frac{A_2}{A_F}. \quad (4)$$

The grid transmissions are T_{G_0}, T_{G_1} and T_{G_2}, respectively. The collisional transmission T_{GAP} of the 239 μm inter-grid gaps is assumed equal for each gap and is calculated from the gap width w, the neutral density, N, at the working pressure and σ, the sum of the ion–atom charge transfer and elastic collision cross-sections (3.9×10^{-19} m^2) [14, 16].

$$T_{GAP} = e^{-\sigma N w}. \quad (5)$$

The unknowns in equations (1), (2), (3), (4) and (5) are the grid transmissions T_{G_0}, T_{G_1} and T_{G_2} and the top face SE emission coefficient γ. The equations were solved for the four unknown variables, assumed initially to be pressure-dependent, using a least squares method to give the best fits. The initial fit showed three parameters, T_{G_1}, T_{G_2} and γ to be remarkably independent of pressure. The fitting was thus repeated using pressure-independent values for these three parameters and a pressure-dependent T_{G_0}. The results of these fits are plotted (solid lines) in figure 8. The pressure-independent values were $T_{G_1} = 0.32$, $T_{G_2} = 0.32$ and $\gamma = 0.1$. The value of T_{G_0} fell from ~ 0.24 at 0.5 mTorr to an equilibrium level of $\sim$0.15 for pressures above 10 mTorr (figure 10). Several factors could lead to the observed T_{G_0} dependence with pressure, in particular beam divergence and beam plasma. At higher pressures, ion–neutral collisions will increase the ratio of divergent beam ions to those on or near the beam axis. This increased proportion of divergent ions will not be collected due to the finite angular acceptance of the RFEA, causing the observed drop in current.

A visible beam plasma is always associated with the ion beam, and is caused by two electron production processes: SEs

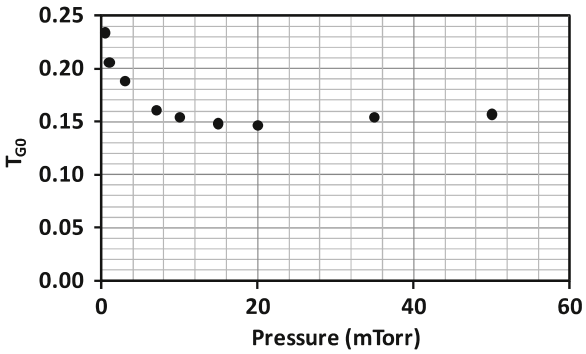

Figure 10. Pressure T_{G_0}, derived from least squares fit.

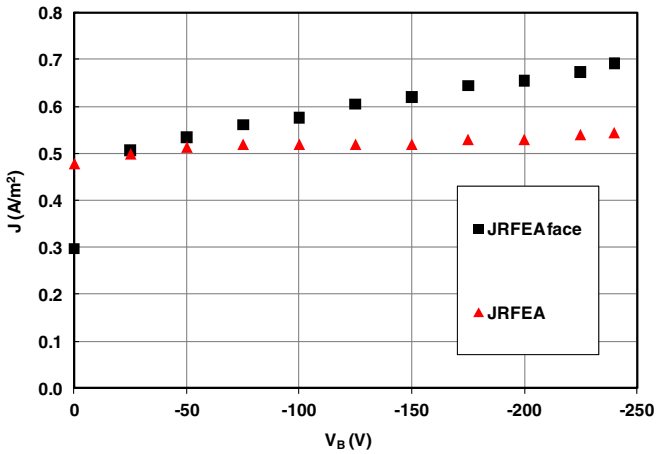

Figure 11. Variation of current density at the RFEA top face and calculated from I_C versus V_B.

released from the table/RFEA and ion–neutral ionization along the ion beam path. In both cases electrons are accelerated by the bias voltage back along the beam axis causing further ionization through collisions with residual gas; beam plasma density thus increases with pressure. The measured RFEA top face current I_F thus contains a pressure-dependent component of slow beam plasma ions. This gives an overestimation of I_F and thus apparent reduction of T_{G_0} with increasing pressure. Indeed this beam plasma effect can be so great that I_F increases significantly with V whilst I_C is near constant (figure 11). We see that the current density calculated from the measured collector current and transparencies is nearly constant over a wide range of bias voltage whereas that determined from the RFEA top face shows a steady increase with V_B due to beam plasma and acceptance effects.

4. Discussion

4.1. Calculated grid transparencies

Grid transparencies T_{G_1} and T_{G_2} obtained using least squares fits were pressure-invariant and equal at 0.32, very close to the estimated optical transmission $T_{OPT} = 0.34$. The similar and pressure-independent values of T_{G_1} and T_{G_2} are most probably due to ion optics within the RFEA. We observe ion transmissions T_{G_1} and $T_{G2} \sim T_{OPT}$ and are not sensitive to experimental conditions. This indicates that the net divergence of a beamlet passing through an individual orifice is sufficient to spread that beamlet over many orifices at a subsequent grid. Several factors could play a part in beamlet spread and steering: ion beam effects, ion optical effects, collisions, grid geometry and grid misalignment. Detailed consideration of these factors indicates that the net divergence required for this spread is due to the combined effects of non-normal incidence due to electric field or beam plasma sheath distortion above G_0, grid geometry and alignment, individual beamlet divergence and ion lens aberrations particularly at G_0. It was necessary to vary T_{G_0} with pressure in order to obtain a best fit. This is not surprising because unlike currents I_{G_1} and I_{G_2}, the current I_{G_0} results from complex pressure-dependent components such as slow beam plasma ions and subsequent SE production. In addition, measurement of ion current at the top face is unrestricted by acceptance angle, and there may be a change in ion angular distribution with pressure.

4.2. Calibrated collector current

The ion current density (J_i) can be calculated from the collector current (I_C) using the following equation and the values T_{GAP}, T_{G_0}, T_{G_1} and T_{G_2} obtained in section 3:

$$J_i = \frac{I_C}{T_{GAP}^3 \cdot T_{G_0} \cdot T_{G_1} \cdot T_{G_2} \cdot A_{G0}}.$$

For example, given that T_{G_1} and T_{G_2} are constant at ~0.32, J_i calculated using $I_C = 200$ nA obtained from figure 4 and the T_{G_0} and T_{GAP} values for 1 mTorr:

$$J_i = 0.5 \frac{A}{m^2}.$$

This calibration is valid for the RFEA under argon ion beam processing conditions, described in section 2. If this RFEA were to be calibrated for a different process, e.g. an ICP plasma, we assume the calculated values of T_{G_1} and T_{G_2} will remain constant at 0.32. However, we would expect the value of T_{G_0} to differ, depending on process conditions because the current measured at grid G_0 contains components that are unique to that process (e.g. beam plasma). Thus, a recalculation of T_{G_0} using the method described in section 3 would be necessary. The values for SE emission coefficients determined from the intercepts at −50 V in figure 7 are $\gamma_{Ni} \approx 0.04$ for grid G_2 and $\gamma_{Cu} \approx 0.03$ for the collector. The value for the aluminium top face is $\gamma_{Al} \approx 0.08$. These values are in broad agreement with the literature which shows many 'dirty' metal surfaces have $\gamma \sim 0.1$ for the argon ion energy range investigated [16].

Error analysis shows measurement accuracy is particularly dependent on pressure, with values of ±11% at 0.5 mTorr, ±13% at 5.0 mTorr and ±27% at 50 mTorr. However, while fits to the I_{G_1}, I_{G_2} and I_C data in figure 8 using the function $I = K P^{-1/3}$ also show the scatter rises with pressure, the scatter values are about half the error analysis values. This suggests our error analysis gives overestimates. Calibration using calorimetric methods and/or with pulsed/chopped parallel ion beam would resolve the matter.

5. Conclusions

An RFEA has been calibrated to quantitatively measure ion current arriving from an argon ion beam at pressures from 0.5 to 50.0 mTorr. The difficulty in this type of calibration is in determining with confidence how much ion current is transmitted from the apertures through the RFEA to the collector. A unique method has been presented where the currents generated at each of the retarding grids and the RFEA top surface are measured separately, allowing the reduction in ion current at each grid along the beam path to be monitored and accounted for. A physical model has developed from these I–V measurements which accounts for grid transmissions and pressure-dependent losses within the RFEA. In addition, top face secondary electron emission and collisionality have been addressed. By fitting the collector current to the model, the variability of grid G_0 transmission was found to be the dominant pressure-dependent parameter. This can be attributed to pressure-dependent current components at the top face, namely slow ions from a weak beam plasma and from ions trajectories which fall outside the RFEA orifice angular acceptance. The calibration method developed here allows accurate, quantitative measurement of ion currents for use with RFEAs in higher pressure processes where collisions within the RFEA are expected.

References

[1] Von Keudell A and Jacob W 1997 Interaction of hydrogen plasmas with hydrocarbon films, investigated by infrared spectroscopy using an optical cavity substrate *J. Vac. Sci. Technol.* A **15** 402–7

[2] Baby A, Mahony C M O and Maguire P D 2011 Acetylene–argon plasmas measured at a biased substrate electrode for diamond-like carbon deposition: I. Mass spectrometry *Plasma Sources Sci. Technol.* **20** 015003

[3] Chen Y, Sin K, Jiang H, Tang Y, Sasaki K, Torabi A, Wang L, Park M, Bai D and Shen Y 2007 High moment materials and fabrication processes for shielded perpendicular write head beyond 200 Gb/in^2 *IEEE Trans. Magn.* **43** 609–14

[4] Gahan D, Dolinaj B and Hopkins M 2008 RFEA and Langmuir probe comparison *Plasma Sources Sci. Technol.* **17** 035026

[5] Hopwood J 1993 Ion bombardment energy distributions in a radio frequency induction plasma *Appl. Phys. Lett.* **62** 940

[6] Edelberg E A, Perry A, Benjamin N and Aydil E S 1999 Energy distribution of ions bombarding biased electrodes in high density plasma reactors *J. Vac. Sci. Technol.* A **17** 506

[7] Mizutani N and Hayashi T 2001 Ion energy and angular distribution at the radio frequency biased electrode in an inductively coupled plasma apparatus *J. Vac. Sci. Technol.* A **19** 1298

[8] Mizutani N and Hayashi T 2000 Ion energy distribution at an rf-biased electrode in an inductively coupled plasma affected by collisions in a sheath *Thin Solid Films* **374** 167

[9] Mizutani N, Nagata Y, Kubo A and Hayashi T 1998 Ion energy and mass analyzer at radio frequency electrode in a plasma chamber *Rev. Sci. Instrum.* **69** 1918

[10] Gahan D, Dolinaj B and Hopkins M 2008 Retarding field analyzer for ion energy distribution measurements at a radio-frequency biased electrode *Rev. Sci. Instrum.* **79** 033502

[11] Denieffe K, Mahony C M O, Maguire P D and Baby A 2011 CoFe and NiFe alloy sputter yield measurements (to be submitted)

[12] Palmer M, Billing M, Calvey J, Codner G, Greenwald S, Li Y, Liu X, Livezey J, Meller R and Schwartz R 2009 Design Implementation and first results of retarding field analyzers developed for the CESRTA program (ID: TH5RFP030) *Proc. PAC09 (Vancouver, 4–8 May 2009)*

[13] Baloniak T, Reuter R, Flötgen C and von Keudell A 2010 Calibration of a miniaturized retarding field analyzer for low-temperature plasmas: geometrical transparency and collisional effects *J. Phys. D: Appl. Phys.* **43** 055203

[14] Phelps A 1991 Cross sections and swarm coefficients for nitrogen ions and neutrals in N_2 and argon ions and neutrals in Ar for energies from 0.1 eV to 10 keV *J. Phys. Chem. Ref. Data* **20** 557

[15] http://www.impedans.com/semion.html

[16] Phelps A and Petrovic Z L 1999 Cold-cathode discharges and breakdown in argon: surface and gas phase production of secondary electrons *Plasma Sources Sci. Technol.* **8** R21–44